

PACS numbers: 42.55.Px; 42.60.Jf; 42.60.Lh
DOI: 10.1070/QE2014v044n02ABEH015251

Simulation of power–current characteristics of high-power semiconductor lasers emitting in the range 1.5–1.55 μm

P.V. Gorlachuk, A.V. Ivanov, V.D. Kurnosov, K.V. Kurnosov,
V.I. Romantsevich, V.A. Simakov, R.V. Chernov

Abstract. **We report the simulation of power–current characteristics of high-power semiconductor lasers emitting in the range 1.5–1.55 μm. A technique is described which allows one to determine the thermal resistance and characteristic temperatures of a laser diode. The radiative and nonradiative carrier recombination rates are evaluated. Simulation results are shown to agree well with experimental data.**

Keywords: *power–current characteristic, spectral range 1.5–1.55 μm, thermal resistance, radiative and nonradiative carrier recombination.*

1. Introduction

Power–current (P–I) characteristics of high-power semiconductor lasers have been the subject of extensive studies. A review by Tarasov [1] and references therein present their results for both cw and pulsed laser operation and formulate relevant implementation concepts. High-power semiconductor lasers emitting in the range 1.5–1.55 μm were studied in Refs [2–6].

In what follows, high-power semiconductor lasers are taken to mean lasers with a contact width of at least 50 μm, which considerably exceeds that of lasers used in optical information transfer (1.5–3 μm). High pump currents lead to severe heating of the active region of laser diodes (LDs). The P–I behaviour of lasers emitting in the range 1.5–1.55 μm is the most difficult to analyse. The strong temperature dependence of their output power is due to Auger recombination processes, radiative and nonradiative recombination processes in the waveguide layers and carrier leakage, which lead to saturation of their P–I characteristic with increasing pump current [7, 8].

In this paper, we demonstrate how to determine the key characteristics of an emitter from its P–I and current–voltage (I–V) characteristics at different fixed temperatures of the heat sink it is mounted on.

P.V. Gorlachuk, A.V. Ivanov, V.D. Kurnosov, K.V. Kurnosov, V.I. Romantsevich, V.A. Simakov, R.V. Chernov OJSC M.F. Stel'makh Polyus Research Institute, ul. Vvedenskogo 3/1, 117342 Moscow, Russia; e-mail: gorlachuk@bk.ru, mail@dilas.ru, webeks@mail.ru

Received 5 June 2013; revision received 21 June 2013
Kvantovaya Elektronika **44** (2) 149–156 (2014)
Translated by O.M. Tsarev

2. Parameters of heterostructures and lasers

The $Ga_yAl_xIn_{1-x-y}As/InP$ heterostructures under consideration had two 90 Å thick quantum wells (QWs). The QWs were separated by a 130 Å thick barrier layer and adjoined waveguide layers 0.65 and 1 μm in thickness (in choosing the geometry and doping level of the layers in the heterostructure, we relied on the broad asymmetric waveguide configuration [9]). The active regions, barriers and waveguide layers were undoped.

The heterostructures were used to fabricate mesa stripe LDs with a stripe contact width of 100 μm. The LD cavities were 1600 and 2000 μm in length. The cavity facets had high-reflectivity (100%) and anti-reflection (5%) coatings.

The laser diodes were soldered, with their active region down, onto contact plates. Each plate was then placed in an 11-mm-diameter cylindrical housing. The housing was mounted on a heat sink, which was maintained at constant temperature ($T = T_0 + \Delta T$, $T_0 = 20\,^\circ$C, $\Delta T = 0$, 5 or 10 °C) using an electronic stabilisation circuit. P–I and I–V measurements were made at a constant pump current.

3. Calculated relationships for determining the thermal resistance and characteristic temperatures of the LDs

The output power of an LD is [10]

$$P = \hbar\omega n_{\rm ph} f V_{\rm a}, \tag{1}$$

where $\hbar\omega$ is the photon energy; $n_{\rm ph}$ is the photon density in the LD cavity; $f = c\alpha_{\rm m}$ is the diode output function; $\alpha_{\rm m} = L^{-1}\ln(R_1R_2)^{-1/2}$; c is the group velocity; L is the cavity length; R_1 and R_2 are the reflectivities of the mirrors; and $V_{\rm a}$ is the volume of the active region.

Neglecting the contribution of spontaneous emission to the lasing mode, we obtain from steady-state solutions to rate equations [11, 12]

$$\frac{I\eta_{\rm in}}{qV_{\rm a}} = \frac{n_{\rm a}}{\tau} + \frac{n_{\rm ph}}{\tau_{\rm ph}}, \tag{2}$$

where I is the pump current; $n_{\rm a}$ is the carrier concentration in the QWs; $\eta_{\rm in}$ is the injection efficiency, which shows which fraction of the pump current reaches the QWs; τ is the carrier lifetime with allowance for radiative and nonradiative recombination; q is the electron charge;

$$\tau_{ph} = [c(\alpha + \alpha_m)]^{-1} \quad (3)$$

is the photon lifetime in the cavity; and α is the loss due to free carriers in the LD cavity.

Equation (1) can be written in the form

$$P = \eta_{t00}(I - I_{t00}), \quad (4)$$

where

$$\eta_{t00} = \hbar\omega q^{-1}\eta_{in}\eta_r \quad (5)$$

is the efficiency (slope) of the $P-I$ characteristic with no allowance for active-region heating;

$$\eta_r = \frac{\alpha_m}{\alpha + \alpha_m} \quad (6)$$

is the efficiency of the resonator; and

$$I_{t00} = \frac{qV_a}{\eta_{in}}\frac{n_a}{\tau} \quad (7)$$

is the threshold current for lasing with no allowance for active-region heating. Taking into account (5) and (6), we obtain

$$\frac{h\omega}{q}\frac{1}{\eta_{t00}} = \frac{1}{\eta_{in}}\left(1 + \frac{\alpha}{\alpha_m}\right). \quad (8)$$

When the heating of the active region by the threshold current is taken into account, the expressions for the efficiency of the $P-I$ characteristic and the threshold current take the form

$$\eta_{t0} = \eta_{t00}(T_0)\exp\left(\frac{-R_T U_{t0} I_{t0}}{T_P}\right), \quad (9)$$

$$I_{t0} = I_{t00}(T_0)\exp\left(\frac{R_T U_{t0} I_{t0}}{T_I}\right), \quad (10)$$

where $U_{t0} = U_{cut} + I_{t0}R_d$ is the threshold voltage of the LD; U_{cut} is the cut-in voltage in the $I-V$ curve; R_d and R_T are the dynamic and thermal resistances of the LD; and T_P and T_I are the characteristic temperatures for the efficiency of the $P-I$ characteristic and the threshold pump current.

$I_{t00}(T_0)$ and $\eta_{t00}(T_0)$ can be compared to analogous quantities for pulsed operation with a low repetition rate of pump current pulses, when active-region heating can be neglected.

The threshold current as a function of pump current and two-facet output power P can be represented in the form [13, 14]

$$I_t(I, P, \Delta T) = I_{t0}(T_0 + \Delta T)\exp\left[\frac{R_T(UI - P)}{T_I}\right], \quad (11)$$

with

$$I_{t0}(T_0 + \Delta T) = I_{t00}(T_0)\exp\left(\frac{\Delta T}{T_I}\right), \quad (12)$$

where ΔT is the change in the temperature of the heat sink and U is the voltage across the LD corresponding to the pump current I. Substituting (10) and (12) into (11), we obtain

$$I_t(I, P, \Delta T) = I_{t0}\exp\left(\frac{\Delta T_{LD}(I, P, \Delta T)}{T_I}\right), \quad (13)$$

where $\Delta T_{LD}(I, P, \Delta T)$ is the heating of the active region. Similarly, we obtain for the efficiency of the $P-I$ characteristic

$$\eta_t(I, P, \Delta T) = \eta_{t0}\exp\left(\frac{-\Delta T_{LD}(I, P, \Delta T)}{T_P}\right). \quad (14)$$

The heating of the active region can be written in the form

$$\Delta T_{LD}(I, P, \Delta T) = R_T(UI - P - U_{t0}I_{t0}) + \Delta T. \quad (15)$$

The LD output power is given by

$$P = \eta_t(I, P, \Delta T)[I - I_t(I, P, \Delta T)]. \quad (16)$$

The thermal resistance RT varies with temperature as [15]

$$R_T(\Delta T_{LD}) = R_{T0}[(T_0 + \Delta T_{LD})/T_0]^k, \quad (17)$$

where k is a constant.

The voltage across the LD,

$$U(I, \Delta T_{LD}) = U_{cut}(\Delta T_{LD}) + IR_d(I) \quad (18)$$

is a nonlinear function of pump current and heating, where

$$U_{cut}(\Delta T_{LD}) = U_{0cut}(1 - dT_u\Delta T_{LD}); \quad (19)$$

$$R_d(I) = R_{d0}(1 - dR_d I); \quad (20)$$

U_{0cut} is the cut-in voltage obtained from a linear fit to the $I-V$ curve at a pump current approaching zero; and dT_u and dR_d are constant coefficients. We take U_{cut} to depend only on temperature, and R_d, only on pump current. (The characteristics of a device whose $I-V$ curve can be represented by a linear function are given in Appendix. In this case, $dT_u = 0$ and $dR_d = 0$.)

Substituting (17) and (18) into (15), we obtain a nonlinear equation in ΔT_{LD}. Solving it, we find ΔT_{LD} as a function of I, P and ΔT.

Substituting (13) and (14) into (16), we obtain a nonlinear equation. Solving it, we find $P = P(I, \Delta T)$, which allows ΔT_{LD}, η_t and I_t to be represented as functions of I, $P(I, \Delta T)$ and ΔT.

Figure 1 shows calculated and experimental $I-V$ and $P-I$ curves for an LD with a cavity length $L = 2000$ μm at different temperatures of the heat sink (20, 25 and 30 °C). The best fit to the experimental data was ensured by adjusting the coefficients in (13)–(20).

Figure 2 shows the heating of the active region, the threshold current and the efficiency of the $P-I$ characteristic as functions of pump current at different heat sink temperatures and $L = 2000$ μm (the characteristics of an LD with $L = 1600$ μm are similar to those in Fig. 2).

All the curves begin at the measured threshold pump currents (see Fig. 1b). Such curves cannot be obtained experi-

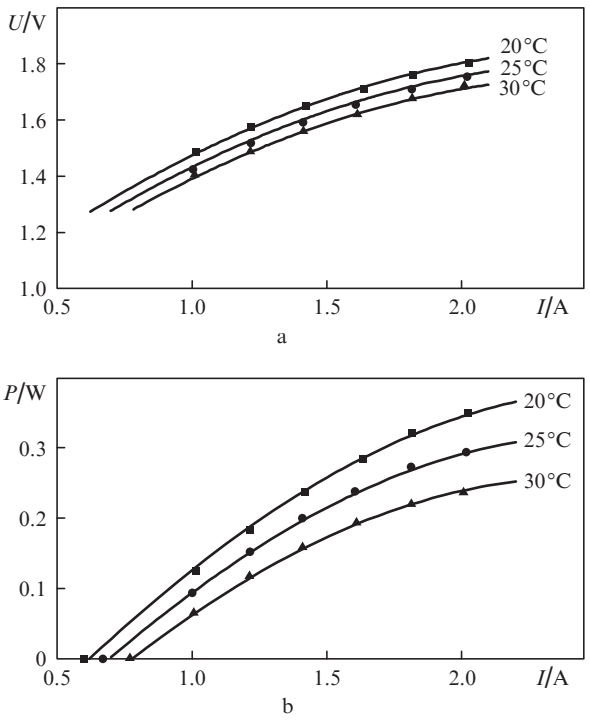

Figure 1. (a) Current–voltage and (b) power–current experimental data (filled symbols) and best fit curves (solid lines) for a laser at heat sink temperatures of 20 (■), 25 (●) and 30 °C (▲).

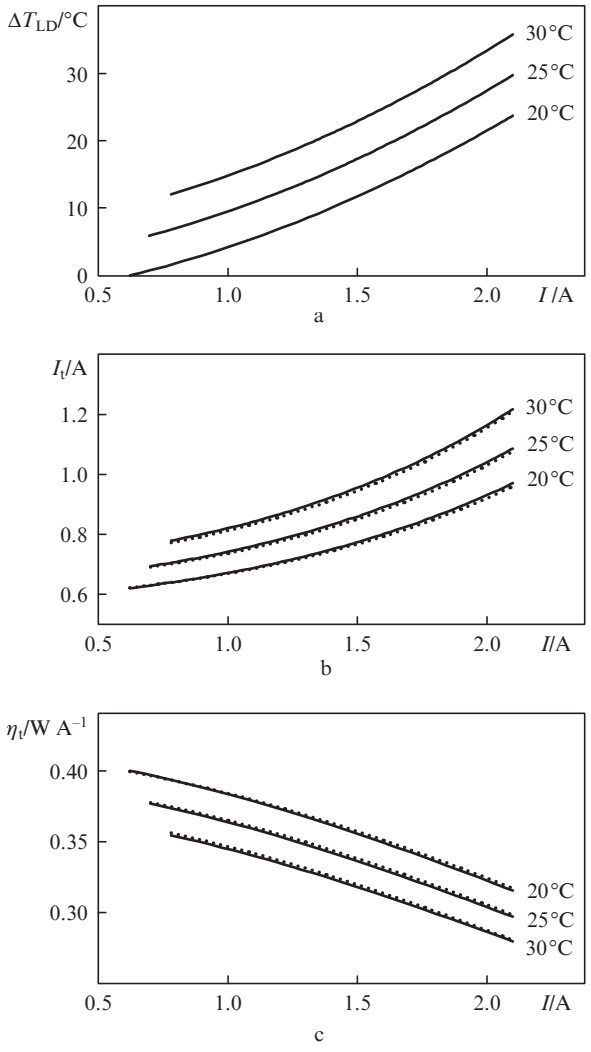

Figure 2. Calculated (a) active region heating, (b) threshold current and (c) threshold efficiency of the $P-I$ characteristic as functions of pump current at heat sink temperatures of 20, 25 and 30 °C. The solid lines represent calculation by Eqns (13)–(15), and the dotted lines represent the best fit curves obtained using Eqns (35) and (36) (see Section 4).

mentally [12, 13]. In particular, as pointed out by Eliseev [12] "the 'threshold' in question cannot be detected by standard means because it varies with output power. In other words, the changed value cannot be measured by reducing the power because this restores its original value." Scott et al. [14] refer to such threshold currents as 'effective'.

It is seen in Fig. 2a that, at a pump current of 2 A, the heating of the active region relative to the heat sink temperature exceeds 20 °C. The plots of the threshold current and efficiency of the $P-I$ characteristic against pump current demonstrate that, with increasing current, the threshold current increases, whereas the efficiency of the $P-I$ characteristic decreases.

Measuring characteristics of LDs at three temperatures in two steps, we were able to determine the thermal resistance of the heat sink. In the first step, after a predetermined pump current was set, we measured the output power of the LD and the voltage across it. Subsequently, the output power gradually decreased because of the heating. In the second step, after the output power reached a steady-state level (3–4 min), the power and voltage were again measured, at the same pump current. The $I-V$ and $P-I$ characteristics obtained in the second step (Fig. 1) are similar to those obtained in the first step. Note that the output power was higher in the first step. In particular, at a pump current of 2 A, it was 0.508, 0.482 and 0.433 W at heat sink temperatures of 20, 25 and 30 °C, respectively. Calculations showed that, in both cases, the characteristic temperatures were identical, and the R_T values were 7 and 2.2 K W^{-1}. The thermal resistance of the heat sink (4.8 K W^{-1}) is the difference between these values.

The value 2.2 K W^{-1} corresponds to the thermal resistance of the interface between the active region and contact plate, and 7 K W^{-1} is the thermal resistance of the interface between the active region and heat sink (together with the LD housing). We were able to determine the thermal resistance of the heat sink (4.8 K W^{-1}) because the temperature sensor was located directly on the heat sink.

The best fit curves in Fig. 1 were obtained at $T_I = 53$ K, $T_P = 100$ K, $R_T = 7$ K W^{-1}, $R_{d0} = 0.8$ Ω, $dT_u = 0.0095$ K^{-1}, $dR_d = 0.14$ A^{-1}, $U_{cut} = 0.82$ V, $I_{t0} = 0.62$ A and $\eta_{t0} = 0.4$ W A^{-1}.

Zegrya et al. [6] obtained $T_I = 60$ K, and Sayid et al. [16] reported $T_P = 91$ K, which correlates with our results.

Satisfactory agreement between the calculation results and experimental data in Fig. 1 takes place only when the indicated quantities deviate by no more than 5% (T_P – 10%).

The η_{in} and α were calculated by Eqn (8), η_{t00} was calculated by Eqn (9), U_{t0} and I_{t0} were determined from experimental data, and R_T and T_P were adjusted so as to ensure the best fit to the $I-V$ and $P-I$ experimental data. At $L = 1600$ and 2000 μm, calculation gives $\alpha = 1.3$–1.5 cm^{-1} and $\eta_{in} = 0.62$. If η_{t00} is replaced by η_{t0} in (8), α and η_{in} become negative at $L = 1600$ μm because of the stronger active-region heating.

Since η_t and I_t depend on output power, the experimentally determined differential efficiency of the $P-I$ characteristic, $\eta_d(I,\Delta T) = dP/dI$, will differ from the efficiency $\eta_t(I,\Delta T)$.

Indeed, with increasing pump current (due to active-region heating), the efficiency η_d begins to decrease, down to negative values, whereas $\eta_t(I,\Delta T)$ is always greater than zero.

Equating the derivative of (16) with respect to dI to zero, we can find the maximum output power and the pump current above which the power decreases.

The relations between η_t and η_d in the case when $I-V$ data can be represented by a linear function are given in Appendix.

4. Calculation of the radiative and nonradiative carrier recombination rates

In calculations, we will use earlier results [17–22]. As shown by Ivanov et al. [18], the best agreement between theory and experiment is ensured by models without mass inversion, with radiative transitions that violate selection rules.

In calculating size quantisation levels, we will use longitudinal components of heavy hole masses:

$$m_{hhi} = \frac{m_0}{\gamma_{1i} - 2\gamma_{2i}}, \tag{21}$$

where i = a (active region) or w (waveguide layers). The Luttinger–Kohn parameters γ_{1i} and γ_{2i} were evaluated using the interpolation formulas

$$\gamma_1(Ga_yAl_xIn_{1-x-y}As) = \gamma_1(InAs)(1-x-y) + \gamma_1(GaAs)y + \gamma_1(AlAs)x, \tag{22}$$

where the γ_1 values for InAs, GaAs and AlAs were taken from Table 1 in Ref. [21]. In a similar way, we evaluated γ_2. The electron effective mass was determined using a formula analogous to (22). The band gap $E_g(T)$ of $Ga_yAl_xIn_{1-x-y}As$ layers was calculated using Eqns (A2)–(A5) in Appendix. We took into account the pump-current-induced decrease in the band gap of the active region:

$$E_{ga} = E_{ga}(T) - k_g(n_a^{1/3} + p_a^{1/3}), \tag{23}$$

where n_a and p_a are the electron and hole concentrations in the QWs; k_g is a constant; and $E_{ga}(T)$ was evaluated using Eqns (A2)–(A5).

The conduction band offset ΔE_c was taken to be $0.72\Delta E_g$, where ΔE_g is the band gap mismatch between the active region and waveguide layers [20]. The refractive indices of the solid solutions, $n(\hbar\omega)$, were calculated using Eqn (2) in Ref. [23]. The optical confinement factors of the two QWs, $\Gamma_a = 0.011$, and waveguide, $\Gamma_w = 0.94$, were thought to be constant, independent of temperature and carrier concentration.

When the wave vector selection rule is not fulfilled, the gain coefficient with allowance for transitions between the first quantum level in the conduction band, ε_{e1}, and the first quantum level for heavy holes in the valence band, ε_{hh1}, can be written in the form

$$g(\hbar\omega) = G_0 \times \ln\left\{\frac{[1 + a_1\exp(-\hbar\omega/(k_BT))][1 + b_1\exp(\hbar\omega/(k_BT))]}{a_2b_2}\right\}, \tag{24}$$

where $a_1 = \exp[(F_c - \varepsilon_{hh1})/(k_BT)]$; $b_1 = \exp[(F_v - E_{ce1})/(k_BT)]$; $a_2 = 1 + \exp[(F_c - E_{ce1})/(k_BT)]$; $b_2 = 1 + \exp[(F_v - \varepsilon_{hh1})/(k_BT)]$; the coefficient G_0 is defined by Eqn (23) in Ref. [18]; and $E_{ce1} = E_{ga} + \varepsilon_{e1}$.

The maximum photon energy corresponding to the maximum gain coefficient is determined by the condition $dg(\hbar\omega)/d\hbar\omega = 0$:

$$\hbar\omega_{max} = \frac{1}{2}[(E_{ce1} + \varepsilon_{hh1}) + (F_c - F_v)]. \tag{25}$$

It is related to the electron and hole concentrations in the QW active region by

$$\hbar\omega_{max} = E_{ce1} + \varepsilon_{hh1} + \frac{1}{2}k_BT \times \ln\left\{\left[\exp\left(\frac{n_a}{\rho_e k_BT}\right) - 1\right]\left[\exp\left(\frac{p_a}{\rho_v k_BT}\right) - 1\right]\right\}, \tag{26}$$

where $\rho_e = m_{ca}/(\pi\hbar^2 L_a)$; $\rho_v = m_{hha}/(\pi\hbar^2 L_a)$; m_{ca} and m_{hha} are the electron and heavy hole effective masses in the QWs; and L_a is the QW width.

The maximum gain coefficient $g_{max} = G_0\ln[(1 + \sqrt{a_1b_1})^2 \times (a_2b_2)^{-1}]$ can be expressed through the electron and hole concentrations in the QW active region in the form

$$g_{max} = G_0\left[\frac{n_a}{\rho_e k_BT} + \frac{p_a}{\rho_v k_BT} - 2\ln\left(\sqrt{\exp\left(\frac{n_a}{\rho_e k_BT}\right) - 1} + \sqrt{\exp\left(\frac{p_a}{\rho_v k_BT}\right) - 1}\right)\right]. \tag{27}$$

The electron and hole concentrations in the waveguide can be expressed through those in the active region of the LD:

$$n_w = N_{cw}\exp\left(-\frac{\Delta E_c - \varepsilon_{e1}}{k_BT}\right)\left[\exp\left(\frac{n_a}{\rho_e k_BT}\right) - 1\right], \tag{28}$$

$$p_w = N_{vw}\exp\left(-\frac{\Delta E_v - \varepsilon_{hh1}}{k_BT}\right)\left[\exp\left(\frac{p_a}{\rho_v k_BT}\right) - 1\right], \tag{29}$$

where $N_{cw} = 2[(m_{cw}k_BT)/(2\pi\hbar^2)]^{3/2}$; $N_{vw} = 2[(m_{hhw}k_BT)/(2\pi\hbar^2)]^{3/2}$; m_{cw} and m_{hhw} are the electron and hole effective masses in the waveguide; and ΔE_c and ΔE_v are the conduction band and valence band offsets.

The electron and hole concentrations in a laser active region containing M_{qw} QWs are related to those in the waveguide by the electroneutrality condition [24]

$$M_{qw}L_a(n_a - p_a) + L_w(n_w - p_w) = 0, \tag{30}$$

where L_w is the waveguide width.

The condition for lasing in the LD has the form

$$\Gamma_a g_{max} = L^{-1}\ln(R_1R_2)^{-1/2} + \Gamma_a\alpha_a + \Gamma_w\alpha_w + (1 - \Gamma_a - \Gamma_w)\alpha_{em}. \tag{31}$$

The losses due to free carriers in the active region, waveguides and emitters are given by

$$\alpha_i = \sigma_e n_i + \sigma_h p_i, \tag{32}$$

where i = a, w or em; n_i and p_i are the carrier concentrations in the layers of the structure (n_{em} and p_{em} are determined by the doping level in the n- and p-emitters); and σ_e and σ_h are the electron and hole absorption cross sections. Scattering losses are neglected in Eqn (32).

Following Grinberg [25], we represent the spontaneous recombination rates in the QWs and waveguide in the following form:

$$R_{spa} = B_{spa}\left(\frac{T_0}{T_0 + \Delta T_{LD}}\right) n_a p_a \left(1 + \frac{n_a + p_a - \sqrt{n_a p_a}}{\mathcal{N}_a}\right)^{-1}, \tag{33}$$

$$R_{spw} = B_{spw}\left(\frac{T_0}{T_0 + \Delta T_{LD}}\right)^{3/2} n_w p_w \left(1 + \frac{n_w + p_w - \sqrt{n_w p_w}}{\mathcal{N}_w}\right)^{-1}, \tag{34}$$

where $\mathcal{N}_i = 1/4[(m_{ei} + m_{hhi})k_B T/(\pi\hbar^2)]^{3/2}$; the coefficients B_{spi} are constants; and i = a or w.

The threshold pump current as a function of radiative and nonradiative recombination rates can be written in the form [19, 21]

$$I_t(\Delta T_{LD}) = qV_a\left\{A_n n_a + R_{spa} + C_0 \times \exp\left[\frac{\Delta E}{k_B}\left(\frac{1}{T_0} - \frac{1}{T_0 + \Delta T_{LD}}\right)\right](n_a^2 p_a + n_a p_a^2)\right\}\eta_{in}^{-1}, \tag{35}$$

where $A_n n_a$ is the nonradiative recombination rate; the last term in the brackets is the rate of Auger recombination in the QWs; and the coefficients C_0 and ΔE are constants. A similar relation was used by Minch et al. [21], who proposed a procedure for finding best fit coefficients in fitting experimental data.

Taking into account (13) and (14), we can find a unique correspondence between $\eta_t(\Delta T_{LD})$ and $I_t(\Delta T_{LD})$:

$$\eta_t(\Delta T_{LD}) = \eta_{t0}[I_t(\Delta T_{LD})/I_{t0}]^{-T_l/T_P}. \tag{36}$$

Calculations demonstrate that, if $\eta_t(I, P, \Delta T)$ in (16) is replaced by η_t from (36) and $I_t(I, P, \Delta T)$ is taken in the form (35), we obtain excellent agreement between the calculated and measured P–I characteristics (Fig. 1b), like in the case of calculations by Eqns (13)–(20).

The best fit $I_t(I)$ curves obtained by using Eqn (35) and adjusting the coefficients A_n, B_{spa}, B_{spw}, C_0, ΔE, σ_e and σ_h are presented in Fig. 2b. Similarly, Fig. 2c shows the best fit $\eta_t(I)$ curves obtained by using Eqn (36) and adjusting the relevant coefficients.

The curves presented in Figs 2b and 2c demonstrate satisfactory agreement between the characteristics calculated in the first and second steps of the measurements with the following coefficients: $A_n = 6\times10^7$ s^{-1}, $B_{spa} = 8\times10^{-11}$ cm^3 s^{-1}, $C_0 = 2.6\times10^{-29}$ cm^6 s^{-1}, $\Delta E = 0.18$ eV, $\sigma_e = 3\times10^{-18}$ cm^2, $\sigma_h = 13.4\times10^{-18}$ cm^2 and $B_{spw} = 8\times10^{-11}$ cm^3 s^{-1}. The value $\sigma_e = 3\times10^{-18}$ cm^2 was borrowed from Ref. [22], and $\sigma_h = 13.4\times10^{-18}$ cm^2 was derived from the condition $\alpha = 1.3$ cm^{-1}, obtained previously. A detailed analysis of the internal optical loss in separate confinement quantum well laser heterostructures can be found in Slipchenko et al. [9] and references therein. The loss in a 4-μm-thick asymmetric waveguide (λ = 1.08 μm) was $\alpha = 0.2$ cm^{-1}, and that in a 1.7-μm-thick waveguide was $\alpha = 0.34$ cm^{-1}. In this study, the loss in a 1.65-μm-thick waveguide (λ = 1.5–1.55 μm) is α = 1.3–1.5 cm^{-1}, i.e. about four times higher.

Piprek et al. [19] used the following values in their calculations for $\lambda = 1.3$ μm: $C_0 = 5\times10^{-29}$ cm^6 s^{-1}, $\Delta E = 0.1$ eV, $\sigma_h = 30\times10^{-18}$ cm^2. For the same wavelength, Agrawal and Dutta [10] took $C_0 = 3\times10^{-29}$ cm^6 s^{-1}, $B_{spa} = 1\times10^{-10}$ cm^3 s^{-1} and $A_n = 1\times10^8$ s^{-1}. For $\lambda = 1.5$ μm, Zou and Osinski [26] used $C_0 = 1.3\times10^{-29}$ cm^6 s^{-1}, $B_{spa} = 8\times10^{-11}$ cm^3 s^{-1} and $A_n = 2.2\times10^8$ s^{-1}.

Thus, the coefficients obtained in this study correlate well with previous results.

Figure 3 shows the electron and hole concentrations in the active region and waveguide and the peak emission wavelength λ_{max} as functions of pump current at different heat sink temperatures. All the curves begin at the threshold currents corresponding to Fig. 1b.

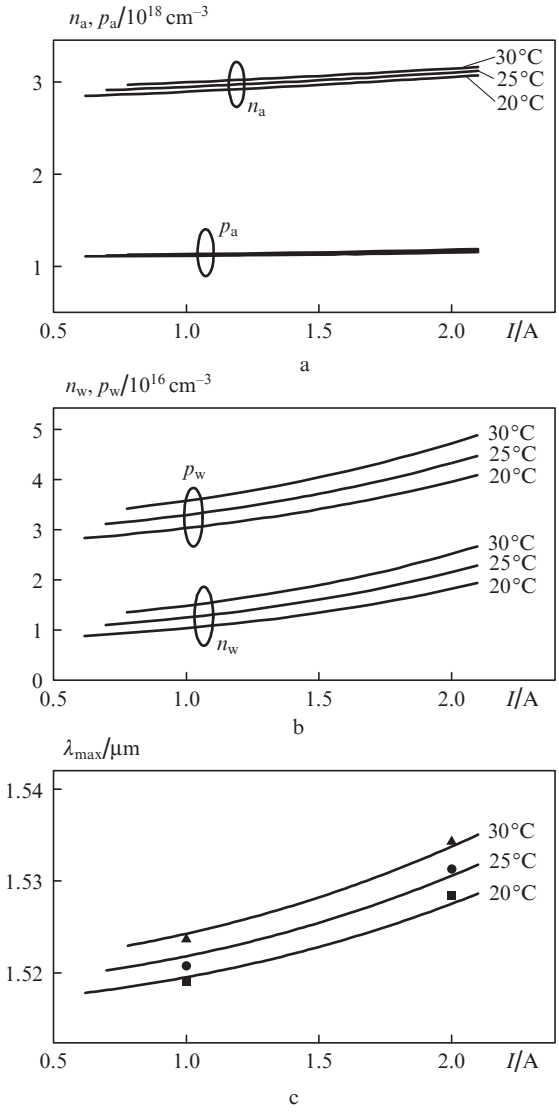

Figure 3. Calculated electron and hole concentrations in the QWs (a) and waveguide (b) and peak emission wavelength (c) as functions of pump current at heat sink temperatures of 20, 25 and 30 °C. The data points represent measured λ_{max} values at heat sink temperatures of 20 (■), 25 (●) and 30 °C (▲).

It is seen that, in both the active region and waveguide, the electron and hole concentrations increase with increasing current. The hole concentration is lower than the electron concentration in the active region and higher in the waveguide. The reason for this is that the barrier to holes is considerably lower than that to electrons ($\Delta E_v/\Delta E_g = 0.28$, $\Delta E_c/\Delta E_g = 0.72$) and, accordingly, the holes more easily diffuse to the waveguide.

The emission wavelength was evaluated as $\lambda_{max} = 1.24/\hbar\omega_{max}$, and $\hbar\omega_{max}$was determined using Eqn (26). Following Ivanov et al. [18], the coefficient k_g in (23) was taken to be 3×10^{-8} eV cm. For comparison, Fig. 3c shows the measured emission wavelength $\lambda_{max}(I)$ at pump currents of 1 and 2 A and heat sink temperatures of 20, 25 and 30 °C. The theoretical predictions and experimental data are seen to be in satisfactory agreement. Note that calculation by Eqns (3)–(13) from Ref. [17] leads to a considerably larger discrepancy between calculation results and experimental data.

The above $\lambda_{max}(I)$ data can be used to evaluate the thermal resistance of the LD, which can be represented in the form $R_T = \Delta T/\Delta P_{diss} = (\Delta\lambda/\Delta T)^{-1}\Delta\lambda/\Delta P_{diss}$, where $\Delta P_{diss} = U_2I_2 - U_1I_1 - \Delta P$ is the power dissipated in the LD; U_2 is the voltage across the LD at a pump current $I_2 = 2$ A; U_1 is the voltage at $I_1 = 1$ A; ΔP is the change in output power at currents of 1 and 2 A. $\Delta\lambda/\Delta T$ was evaluated for pump currents of 1 and 2 A and heat sink temperatures of 20, 25 and 30 °C. The average value is $\Delta\lambda/\Delta T = 5.5$ Å K^{-1} with $\Delta\lambda/\Delta P_{diss} = 40.5$ Å W^{-1}, which yields an estimate $R_T = 7.4$ K W^{-1}. It follows from experimental data that $\Delta\lambda/\Delta T = 5.8$ Å K^{-1}, which gives $R_T = 7$ K W^{-1}, in good agreement with the R_T obtained in Section 3.

Equation (35) gives the threshold current I_t, which includes components determined by radiative and nonradiative recombination processes in the QWs and waveguide, and allows one to find the leakage current:

$$I_{leak} = I_t - I_{spa} - I_{na} - I_A - I_{spw}, \tag{37}$$

where $I_{spa} = qV_aB_{spa}n_ap_a$; $I_{na} = qV_aA_nn_a$; $I_A = qV_aC_0\exp\{\Delta E/k_B[T_0^{-1} + (T_0 + \Delta T_{LD})^{-1}]\}(n_a^2p_a + n_ap_a^2)$; $I_{spw} = qV_w(A_nn_w + B_{spw}n_wp_w)$.

Figure 4a illustrates the effect of heat sink temperature ΔT on the total threshold current I_t calculated by Eqn (35) and its components. It is seen that the largest contribution is made by Auger recombination and leakage currents. Figure 4b shows the leakage current, determined by (37), as a function of heat sink temperature. We failed to account for the obtained I_{leak} by carrier leakage to the emitter in models proposed previously [5, 10, 27, 28]. The reason for this is that the emitters had the composition $Al_{0.48}In_{0.52}As$, with a band gap E_g = 1.45 eV. This is higher by almost $4k_BT$ than the E_g of InP (1.35 eV), which is used in emitters of the InGaAsP/InP system. The leakage currents in the models in question were lower than those in Fig. 4b. Calculations of lateral carrier leakage currents, represented by Eqn (33) in Asryan et al. [29], or carrier spreading currents (see e.g. Joyce [30]) yielded either underestimated leakage currents or inadequate temperature dependences.

An adequate fit to the curves in Fig. 4b can be obtained by calculating the leakage current using a relation from Olshansky et al. [31]:

$$I_{leak} = qV_aDn_a^{5.5} \tag{38}$$

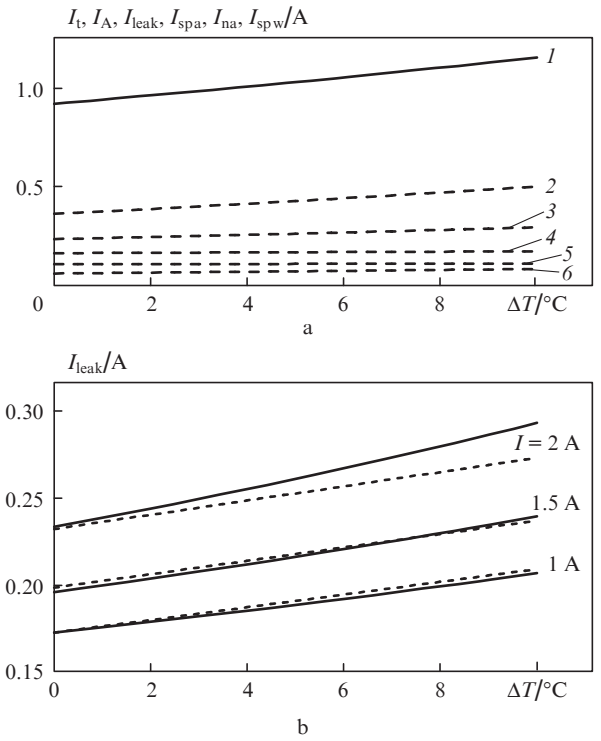

Figure 4. (a) Effect of heat sink temperature on (*1*) the threshold current I_t and its components: (*2*) Auger recombination current I_A; (*3*) leakage current I_{leak}; (*4*) radiative and (*5*) nonradiative recombination currents in the QWs (I_{spa} and I_{na}, respectively); and (*6*) recombination current in the waveguide, I_{spw}. (b) I_{leak} vs. heat sink temperature at pump currents I = 1, 1.5 and 2 A. The solid lines represent calculation by Eqn (37), and the dashed lines represent fits with Eqn (38).

with $D = 8.7\times10^{-76}$ cm$^{13.5}$ s^{-1}. The curves diverge at T = 30 °C as the pump current increases from 1 to 2 A. If calculations use the diffusion component of the leakage current, proportional to $Dn_a^{3.5}$, no agreement between the curves can be reached. Scott et al. [14] represented the leakage current as

$$I_{leak} = j_0wL\exp\left[\frac{-(E_g - \Delta F)}{nk_BT}\right], \tag{39}$$

where j_0 is a fitting parameter; w is the width of the active region; and

$$\Delta F = E_{ce1} + \varepsilon_{hh1} + k_BT \times \ln\left[\left(\exp\left(\frac{n_a}{\rho_e k_BT}\right) - 1\right)\left(\exp\left(\frac{p_a}{\rho_v k_BT}\right) - 1\right)\right] \tag{40}$$

is the difference between the quasi-Fermi levels.

If E_g is taken to be the band gap of the emitter, fitting gives too high a j_0 value. Reasonable results can be obtained if E_g is taken to be the band gap of the waveguide, E_{gw}. All the curves in Fig. 4b are then adequately fitted at $n = 2$ and $j_0 = 6.45\times10^3$ A cm^{-2}. We are thus led to assume that the leakage current is determined by carrier escape from the QW to the waveguide.

In conclusion note that I–V and P–I measurements at three different heat sink temperatures allowed us to determine the characteristic temperatures and thermal resistance of an

LD mounted on a heat sink. Knowledge of R_T (when the same heat sink is used) allows one to monitor the quality of the deposition of Ohmic contacts and the soldering of LDs onto contact plates.

The thermal resistances, characteristic temperatures and radiative and nonradiative carrier recombination rates found in this study ensured adequate agreement between calculation results and experimental data.

Appendix

Figure A1 shows measured and calculated I–V and P–I characteristics for linear current–voltage behaviour. When the voltage across an LD is a linear function of pump current, the differential efficiency of the P–I characteristic can be written in the form

$$\eta_d(I,\Delta T) = \eta_t(I,\Delta T)\left(1+\frac{cb}{a}\right)\left(1+\eta_t\frac{cd}{a}\right)^{-1}, \qquad (A1)$$

where

$$a = 1 - k\left(1+\frac{\Delta T_{LD}}{T_0}\right)^{k-1}\left\{\frac{R_{T0}[(U_{cut}+IR_d)I-P]}{T_0}\right\},$$

$$b = d(U_{cut}+2R_dI),$$

$$c = \frac{-I}{T_P}+\left(\frac{1}{T_P}-\frac{1}{T_I}\right)\exp\left(\frac{\Delta T_{LD}}{T_I}\right),$$

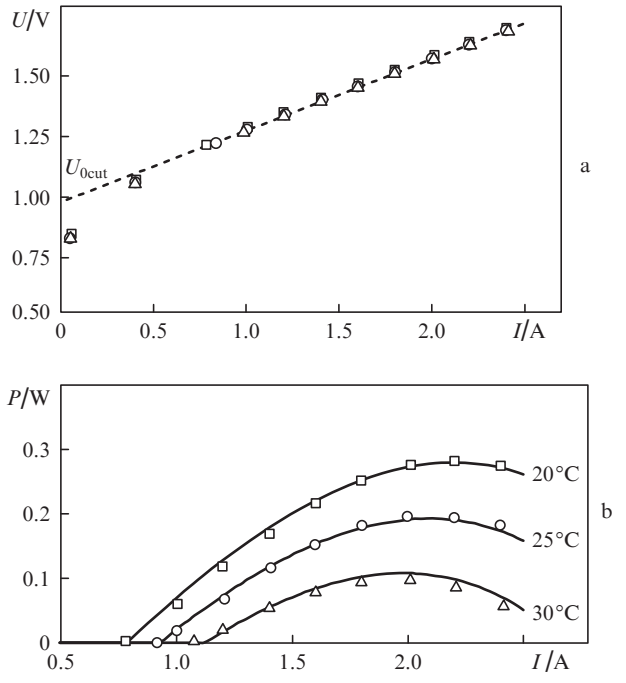

Figure A1. (a) Linearised measured current–voltage and (b) measured power–current characteristics of an LD at heat sink temperatures of 20 (□), 25 (○) и 30 °C (△). The dashed line represents a linear fit to the I–V data, and the solid lines are fits to the P–I data.

$$d = R_{T0}\left(1+\frac{\Delta T_{LD}}{T_0}\right)^k.$$

Determining η_d at a given pump current and ΔT from experimental data, one can evaluate $\eta_t(I,\Delta T)$. Solving the nonlinear equation $1 + cb/a = 0$ in conjunction with (16), one can find the output power and the maximum pump current above which the output power begins to drop.

The experimental data in Fig. A1b demonstrate that the maximum pump current above which the power begins to drop is 1.98, 2.09 and 2.18 A at temperatures of 30, 25 and 20 °C. Calculation yields 1.84, 2.004 and 2.16 A. Given the uncertainty in determining I_{max} from experimental data, the agreement is quite satisfactory.

The temperature dependence of the band gap E_g for $Ga_yAl_xIn_{1-x-y}As$ layers was obtained using Eqn (3) from Ivanov et al. [23]:

$$E_g(Ga_yAl_xIn_{1-x-y}As) = xE_g(AlAs) + yE_g(GaAs)$$

$$+ (1-x-y)E_g(InAs) - xyK_{AlGaAs}$$

$$- y(1-x-y)K_{GaInAs} - x(1-x-y)K_{AlInAs}, \qquad (A2)$$

where $K_{AlGaAs} = 0.399$, $K_{GaInAs} = 0.442$ and $K_{AlInAs} = 0.614$ are nonlinearity parameters of the respective ternary solid solutions, which are thought to be temperature-independent.

The temperature dependences of E_g for the constituent binary solutions were taken from Ref. [17]

$$E_g(InAs) = 0.417 - 2.76\times10^{-4}T^2/(T+93), \qquad (A3)$$

$$E_g(AlAs) = 3.099 - 8.85\times10^{-4}T^2/(T+530), \qquad (A4)$$

$$E_g(GaAs) = 1.519 - 5.405\times10^{-4}T^2/(T+204). \qquad (A5)$$

References

1. Tarasov I.S. *Kvantovaya Elektron.*, **40**, 661 (2010) [*Quantum Electron.*, **40**, 661 (2010)].
2. Boucher J.F., Callahan J.J. *Proc. SPIE Int. Soc. Opt. Eng.*, **8039**, 80390B (2011).
3. Boucher J.F., Vilokkinen V., Rainbow P., et al. *Proc. SPIE Int. Soc. Opt. Eng.*, **7480**, 74800K (2009).
4. Han I.K., Cho S.H., Heim P.J.S., Woo D.H., et al. *IEEE Photonics Technol. Lett.*, **12**, 251 (2000).
5. Skrynnikov G.V., Zegrya G.G., Pikhtin N.A., et al. *Fiz. Tekh. Poluprovodn.*, **37**, 243 (2003).
6. Zegrya G.G., Pikhtin N.A., Skrynnikov G.V., et al. *Fiz. Tekh. Poluprovodn.*, **35**, 1001 (2001).
7. Vinokurov D.A., Kapitonov V.A., Lyutetskiy A.V., et al. *Fiz. Tekh. Poluprovodn.*, **41**, 1003 (2007).
8. Lyutetskiy A.V., Borshchev K.S., Pikhtin N.A., et al. *Fiz. Tekh. Poluprovodn.*, **42**, 106 (2008).
9. Slipchenko S.O., Vinokurov D.A., Pikhtin N.A., et al. *Fiz. Tekh. Poluprovodn.*, **38**, 1477 (2004).
10. Agrawal G.P., Dutta N.K. *Long-Wavelength Semiconductor Lasers* (New York: Van Nostrand, 1986).
11. Tsang W.T. (Ed.) *Semiconductor Injection Lasers* (Orlando: Academic, 1985; Moscow: Radio i Svyaz', 1990).

12. Eliseev P.G. *Vvedenie v fiziku inzhektsionnykh lazerov* (Introduction to the Physics of Injection Lasers) (Moscow: Nauka, 1983).
13. Zholnerov V.S., Ivanov A.V., Kurnosov V.D., et al. *Zh. Tekh. Fiz.*, **82**, 63 (2012).
14. Scott J.W., Geels R.S., Corzine S.W., Coldren L.A. *IEEE J. Quantum Electron.*, **29**, 1295 (1993).
15. Bewtra N., Suda D.A., Tan G.L., Chatenoud F., Xu J.M. *IEEE J. Sel. Top. Quantum Electron.*, **1**, 331 (1995).
16. Sayid S.A., Marko I.P., Cannard P.J., Chen X., et al. *IEEE J. Quantum Electron.*, **46**, 700 (2010).
17. Chang Yi-An, Chen J-R., Kuo H-C., et al. *J. Lightwave Technol.*, **24**, 536 (2006).
18. Ivanov A.V., Kurnosov V.D., Kurnosov K.V., et al. *Kvantovaya Elektron.*, **36**, 918 (2006) [*Quantum Electron.*, **36**, 918 (2006)].
19. Piprek J., White J.K., Thorpe A.J.S. *IEEE J. Quantum Electron.*, **38**, 1253 (2002).
20. Selmic S.R., Chou T.M., Sih J.P., et al. *IEEE J. Sel. Top. Quantum Electron.*, **7**, 340 (2001).
21. Minch J., Park S.H., Keating T., Chuang S.L. *IEEE J. Quantum Electron.*, **35**, 771 (1999).
22. Casey H.C. Jr., Panish M.B. *Heterostructure Lasers* (New York: Academic, 1978; Moscow: Mir, 1981).
23. Ivanov A.V., Kurnosov V.D., Kurnosov K.V., et al. *Kvantovaya Elektron.*, **37**, 545 (2007) [*Quantum Electron.*, **37**, 545 (2007)].
24. Wilcox J.Z., Ou S., Yang J.J., Jansen M., Peterson G.L. *Appl. Phys. Lett.*, **55**, 825 (1989).
25. Grinberg A.A. *IEEE J. Quantum Electron.*, **30**, 1151 (1994).
26. Zou Y., Osinski J.S. *IEEE J. Quantum Electron.*, **29**, 1295 (1993).
27. Garbuzov D.Z., Ovchinnikov A.V., et al. *Fiz. Tekh. Poluprovodn.*, **25**, 928 (1991).
28. Chinn S.R., Zory P.S., Reisinger A.R. *IEEE J. Quantum Electron.*, **24**, 2191 (1988).
29. Asryan L.V., Gun'ko N.A., Polkovnikov A.S., et al. *Semicond. Sci. Technol.*, **15**, 1131 (2000).
30. Joyce W.B. *J. Appl. Phys.*, **51**, 2394 (1980).
31. Olshansky R., Su C.B., Manning J., Powazinik W. *IEEE J. Quantum Electron.*, **20**, 838 (1984).